JACS
JOURNAL OF THE AMERICAN CHEMICAL SOCIETY
Article
pubs.acs.org/JACS

In Situ Visualization of Lithium Ion Intercalation into MoS_2 Single Crystals using Differential Optical Microscopy with Atomic Layer Resolution

Mukkannan Azhagurajan,[†] Tetsuya Kajita,[‡] Takashi Itoh,[‡] Youn-Geun Kim,[§] and Kingo Itaya*[,†,‡]

[†]Institute of Multidisciplinary Research for Advanced Materials, Tohoku University, 2-1-1 Katahira, Sendai 980-8577, Japan
[‡]Frontier Research Institute for Interdisciplinary Sciences (FRIS), Tohoku University, 6-3 Aoba, Sendai 980-8578, Japan
[§]Division of Chemistry and Chemical Engineering, Joint Center for Artificial Photosynthesis , California Institute of Technology, Pasadena, California 91125, United States

Supporting Information

ABSTRACT: Atomic-level visualization of the intercalation of layered materials, such as metal chalcogenides, is of paramount importance in the development of high-performance batteries. In situ images of the dynamic intercalation of Li ions into MoS_2 single-crystal electrodes were acquired for the first time, under potential control, with the use of a technique combining laser confocal microscopy with differential interference microscopy. Intercalation proceeded via a distinct phase separation of lithiated and delithiated regions. The process started at the atomic steps of the first layer beneath the selvedge and progressed in a layer-by-layer fashion. The intercalated regions consisted of Li-ion channels into which the newly inserted Li ions were pushed atom-by-atom. Interlayer diffusion of Li ions was not observed. Deintercalation was also clearly imaged and was found to transpire in a layer-by-layer mode. The intercalation and deintercalation processes were chemically reversible and can be repeated many times within a few atomic layers. Extensive intercalation of Li ions disrupted the atomically flat surface of MoS_2 because of the formation of small lithiated domains that peeled off from the surface of the crystal. The current−potential curves of the intercalation and deintercalation processes were independent of the scan rate, thereby suggesting that the rate-determining step was not governed by Butler−Volmer kinetics.

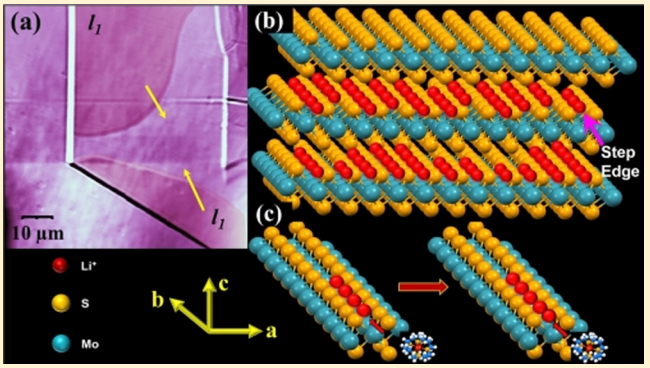

INTRODUCTION

Direct visualization of processes on the electrode surface provides a crucial guide in the rational control and optimization of charge-transfer events. In situ scanning probe microscopic techniques such as scanning tunneling microscopy (STM) and atomic force microscopy (AFM) are well-established techniques that impart atomic-level information of various interfacial phenomena.[1−5] Experimental techniques based on Raman, infrared, and X-ray scattering spectroscopies have been specifically modified also to track the dynamic processes of electrochemical reactions.[6]

STM and AFM studies have been previously applied to the intercalation and deintercalation reactions of Li ions and anions into highly ordered pyrolytic graphite (HOPG).[7−9] Electrochemical deposition of copper and organic molecules into transition-metal dichalcogenides such as TaS_2 has also been investigated, which inferred the formation of nanoscale defects during organic molecule intercalation and deintercalation.[10,11] MoS_2 has been previously studied and employed in many applications, such as catalysis, batteries, and solid lubricants.[12,13] Recently, MoS_2 has attracted much attention in energy storage applications because of its specific physicochemical properties.[13,14] The optical and electrical properties of Li intercalation into MoS_2 nanosheets were also investigated.[15,16]

However, a handful of practical limitations of STM and AFM often curtails the wide applicability of these techniques: (i) The acquisition times, typically in the order of minutes, are known to be inadequate in the evaluation of fast, dynamic processes. Note that a video-rate in situ STM technique has been developed recently to overcome this problem.[17,18] (ii) The small observable scan areas, usually at the submicrometer scale, necessitate the burden of proof that the acquired images statistically represent the entire electrode surface. (iii) STM tips and AFM cantilevers may perturb the concentration distribution of the solute in the vicinity of the electrode surface, thereby leading to, under certain experimental conditions, sluggish electrochemical deposition of metals[19,20] and unfavorable effects during the crystal growth of organic materials.[21]

Received: November 12, 2015
Published: February 16, 2016

DOI: 10.1021/jacs.5b11849
J. Am. Chem. Soc. 2016, 138, 3355−3361

We recently developed a laser confocal microscope combined with a differential interference contrast microscope (LCM−DIM) that can resolve single atomic steps with ca. 0.2−0.3 nm step heights on commonly used metal electrodes. With acquisition times of 2−10 frames per second, the LCM−DIM was shown to capture images of the dynamic electrochemical dissolution and deposition processes on Au(111) surfaces as described in our previous papers.[22,23] Atomically flat surfaces that extended more than a few micrometers were needed to demonstrate clearly the capabilities of the method, because the in-plane resolution resembled that of normal optical microscopes at ca. 0.2−0.3 μm.[22] In this regard, protocols for the preparation of ultraflat Au, Pd, Pt, and Si(100) electrodes were developed.[22−26]

The intercalation of layered materials, such as MoS_2, for charge-storage purposes is an archetypal process that benefits from the direct visualization by LCM−DIM. Efforts to improve the performance of lithium-ion batteries conventionally evaluate current−voltage curves and impedance measurements[12−14] which are devoid of any direct structural information. Elechrochemical STM (EC-STM) has already uncovered important atomic details of the initial stages of lithium-ion intercalation,[7−9] but a complete visualization of the intercalation−deintercalation cycle has never been accomplished. The present report showcases a gallery of LCM−DIM images and videos that reveal the progression of Li-ion intercalation and deintercalation initiated at the monatomic steps of MoS_2 in an ionic liquid. The acquisition of such images with atomic-height resolution has revealed mechanistic insights into the process.

MATERIALS AND METHODS

The LCM−DIM used herein was an improved version of the configuration first reported by Sazaki and co-workers.[21,27] Details of the setup are described in Figures S1 and S2 of the Supporting Information. The acquisition time of each image was typically less than 1 s, depending on the number of data points. The LCM−DIM optics was basically constructed for measurements in air. To achieve atomic-height resolution in solution, a specially designed objective lens (LUCPLAN FLN, Olympus) with a compensator was necessary to account for changes in the refraction index at the solution−glass interface. A high-resolution image of the electrode surface can, therefore, be obtained through a relatively thick layer (<2 mm) formed by the solution and the glass base plate of the electrochemical cell. A more detailed description of the experimental setup is found in Figure S2. AFM images were acquired using a Pico-SPM 5500 (Agilent Corp.). High-resolution STM images were obtained by a NanoScope E (Digital Instruments, Santa Barbara, CA) instrument.

MoS_2 has three well-known polytypes: 1T-MoS_2, 2H-MoS_2, and 3R-MoS_2. X-ray powder diffraction indicated that the MoS_2 sample under investigation had the 2H-MoS_2 structure. The MoS_2 crystals were readily cleaved to expose ultraflat surfaces with terraces wide enough to observe atomic steps clearly with LCM−DIM. The lateral (in-plane) resolution of LCM−DIM was in the range of 0.2−0.3 μm, akin to that of conventional optical microscopes.

Current−potential profiles were acquired using a BAS potentiostat 700D. Details of the electrochemical cell are displayed in Figures S1−S3. An O-ring (Kalrez, Dupon), with outer and inner diameters of 8 and 5 mm, respectively, was placed between the MoS_2 crystal and the electrochemical cell to create a vacuum-tight seal. Li metal was used as a reference electrode. The electrolyte solution consisted of 0.32 mol lithium bis(trifluoromethylsulfonyl)imide (LiTFSI) (Kanto Chem. Co.) per kilogram of 1-ethyl-3-methylimidazolium bis(fluorosulfonyl)-imide (EMI-FSI). To ensure the removal of water, the ionic liquid solution was heated inside the vacuum-tight electrochemical cell at 130 °C using an oil bath for more than 10 h until the pressure was lower than 1×10^{-5} Pascal. A turbo-molecular pump (Pfeiffer Mod. HiCube 80 Classic) was employed to keep the base pressure lower than 10^{-5} Pascal. For LCM−DIM measurements, Au and Teflon meshes were placed between the optically flat glass plate and MoS_2. Details of this configuration are described in Figure S3. For reference purposes, the voltammetric behavior (Figure S4b) of MoS_2 was acquired in a battery-grade electrolyte solution of 1:1 (by volume) ethylene carbonate and diethyl carbonate (Kanto Chem. Co.) containing 1 M $LiClO_4$, without further purification, because most of the previous work on Li-ion batteries used this solvent system.[12,13]

RESULTS

Cyclic Voltammetry of Basal Planes. As-received ionic liquids were found to produce a large cathodic current prior to the onset potential for Li-ion intercalation. For instance, the background current at the potential range between 1.4 and 2.8 V reached ca. 50 μA cm^{-2} at 10 mV s^{-1} (red trace of Figure S4a). Such large background currents were strongly dependent on the concentration of water; preliminary experiments inside a glovebox revealed that the ionic liquid solution contained 20−50 ppm water. The use of rigorously dried solvents dramatically decreased these preintercalation peaks by more than 2 orders of magnitude. Figure S4a indicates that the persistence of broad cathodic peaks should be due to trace amounts of water. A similar small background current has been observed on a HOPG in the same ionic liquid.[28]

In a rigorously dried solvent, the cathodic current for intercalation commenced at a potential of 1.3 V vs Li and increased as the electrode potentials were swept in the negative direction from 3.2 V vs Li, as shown in Figure 1a.

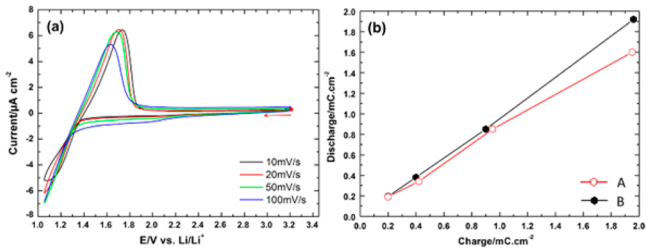

Figure 1. (a) Cyclic voltammograms of a freshly cleaved MoS_2 in a rigorously dried ionic solvent at different scan rates. The electrode potential was scanned from 3.2 V vs Li. (b) Relationship between intercalation and deintercalation charges. The red line (A) shows the raw data without the correction for the small currents between 2.2 and 1.45 V. The black line (B) represents the corrected data.

Deintercalation was induced in the reverse potential scan, giving rise to an anodic peak at ca. 1.6 V. These experiments demonstrated the chemical reversibility of the intercalation and deintercalation processes.

Surprisingly, both anodic and cathodic currents did not vary significantly with the scan rates between 10 and 100 mV s^{-1}. The diffusion of Li ions into the MoS_2 sheets was, therefore, non-Fickian, otherwise the currents would have been proportional to the square root of the scan rate. At the lowest scan rate of 10 mV s^{-1} (black trace in Figure 1a), a small cathodic current appeared at ca. 2.2 V. At a potential range of 1.1−1.3 V, the intercalation current was almost linearly dependent on the potential. The Butler−Volmer equation predicts an exponential dependence of current on potential for electrode processes controlled by electronic charge transfer.

Figure 1b depicts the relationship between the total charges associated with the intercalation and deintercalation processes.

DOI: 10.1021/jacs.5b11849
J. Am. Chem. Soc. 2016, 138, 3355−3361

Line A represents measured charges without background correction. According to this line, only ca. 80% of doped Li ions were deintercalated. A close scrutiny of Figure 1a indicated small cathodic currents (<1 μA cm^{-2}) between the onset potential for intercalation and 2.2 V; such small currents were ascribed to the reduction of trace amounts of water or unknown organic impurities.

Control experiments were conducted in LiTFSI-free solvents to ascertain background-charge contributions. Background-correct charges (line B) revealed that nearly all of the intercalated Li ions were involved during the charging–discharging processes. For 2H-MoS_2 crystal, the maximum charge density for a single monolayer is 0.185 mC cm^{-2}, calculated from the structure of 2H-MoS_2. This value corresponds to the theoretical specific charge capacity of 167 mAh g^{-1}.[12,29] The highest charge density measured in the experiments shown in Figure 1b was 2 mC cm^{-2}, which was obtained at a scan rate of 10 mV s^{-1}; this charge corresponded to the intercalation of ca. 10 monolayers.

LCM–DIM Images. MoS_2 crystals can be cleaved easily by an adhesion tape (such as Scotch tape). Surfaces cleaved in this manner usually showed many step lines and atomically flat regions with narrow widths. Ultraflat wide surfaces, however, can be exposed by the placement of the crystal between, and its subsequent detachment from, two glass plates each stuck with an instant adhesive. LCM–DIM images of perfectly cleaved MoS_2 samples (Figure S5) clearly show well-defined ultraflat surfaces with only monatomic steps.

Figure 2a,b shows two typical wide-scan images (140 × 140 μm^2) acquired by LCM–DIM in air. The surfaces were remarkably flat, and the terraces were more than several micrometers wide. Notably, the MoS_2 sample was polycrystalline, but single-crystal domains were obviously large. All step lines formed during cleavage were random and showed no preferential direction with respect to the crystal structure. Large pits surrounded by monatomic steps, such as those bordered by the dashed circle S_1 in Figure 2a, originated from wide terraces that were partially peeled off during the cleaving process.

Monoatomic steps typically registered an atomic height of 0.6 nm. Some monatomic steps (S_1 in Figure 2b) were found to extend more than 100 μm across the surface. Diatomic (S_2) and multiatomic steps (S_3 and S_5) were also found in different areas. It is noteworthy that when the step height was smaller than the wavelength of the laser, the contrast (brightness) of these steps almost scaled linearly with the step height. Such linearity was confirmed by the comparison between LCM–DIM and STM/AFM images.

STM Images. Verification of the step heights observed by LCM–DIM was accomplished by the re-examination of the same samples with EC-STM operated in air. Figure 3 displays two typical STM images. Height profiles along lines drawn in each STM image are shown in panels a′ and b′ of Figure 3. Figure 3a shows an atomically flat terrace with a step height of ca. 0.62 nm, which was consistent with the literature value of the height of the unit cell in the *c*-axis of 2H-MoS_2.[12,13]

Figure 3b displays a surface with several steps of different atomic heights. The S_1 and S_2 arrows indicate monatomic and diatomic steps, respectively. The coalescence of two diatomic steps gave rise to a step (S_4) that is four atoms high.

A careful inspection of the high-resolution STM images of the terraces in Figure 3b revealed regular lines with height differences (ca. 0.1–0.2 nm) smaller than a monatomic step height (ca. 0.62 nm). Details from Figure S6a,b showed that these line features constituted steps with submonoatomic heights.

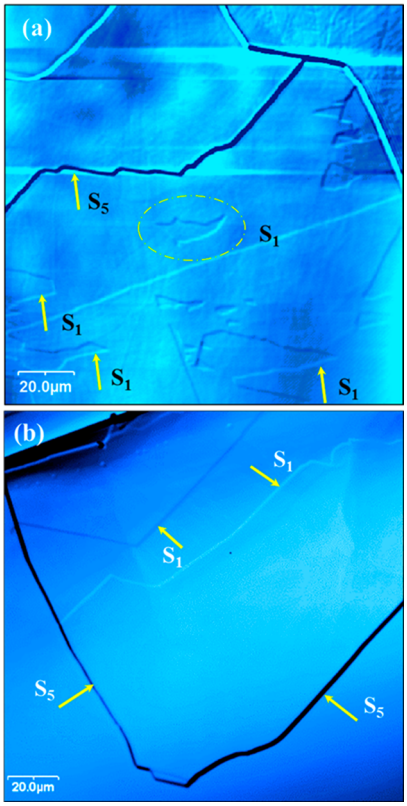

Figure 2. Typical LCM–DIM images of freshly cleaved surfaces observed in air. The size of the observed areas were 140 × 140 μm^2. Both images show very wide terraces with mostly monatomic steps (S_1); steps with multiatomic heights, such as S_5, can also be found. (a) Basin-shaped pits surrounded by monatomic steps are indicated by the dashed circle, S_1. (b) Two monatomic step lines marked by S_1 are relatively straight and extended more than 100 μm across the surface. All images were taken in a large area of 140 × 140 μm^2.

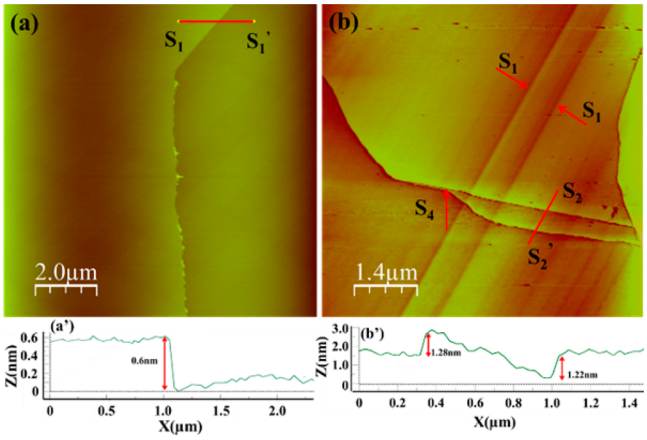

Figure 3. High-resolution STM image of MoS_2 in ionic liquid at a potential of 3.0 V. The tunneling current was 5 nA. (a) The height profile along a line S_1–S_1′ indicated that the step is monatomic with height of ca. 0.62 nm, as shown in panel a′. (b) The height profile along a line S_2–S_2′ revealed the presence of diatomic steps, as shown in panel b′. These diatomic steps coalesced at point S_4 to form a step that was four-atoms high. The images of panels a and b were taken in an area of 10 × 10 μm^2 and 7 × 7 μm^2, respectively.

DOI: 10.1021/jacs.5b11849
J. Am. Chem. Soc. 2016, 138, 3355–3361

Intercalation and Deintercalation in the First Monolayer Underneath the Selvedge. A slow potential sweep (scan rate = 10 mV s^{-1}) headed in the negative direction from 3.2 V vs Li immediately gave rise to a cathodic current at 1.3 V that marked the intercalation of Li ions into the MoS_2 crystal. At the incipient stage of intercalation, when the current density was only ca. 1−2 $\mu A\,cm^{-2}$ (1.25 V vs Li), the electrode potential was fixed and a series of LCM−DIM images (Figure 4a−c) was acquired. Note that in order to see two phases clearly, a data treatment was applied with high contrast ratio. In this case, terraces seemed to be not very flat, showing rolling hill structures. This structure might be an artifact caused by the present data treatment. A similar irregular structure can also be seen in Figure 2a.

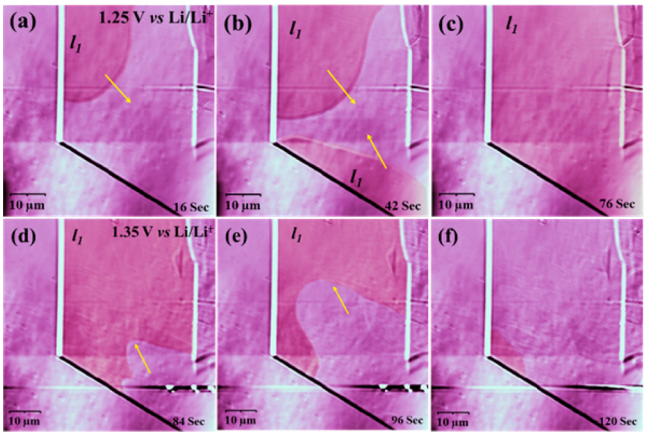

Figure 4. Dynamic processes of intercalation (a−c) and deintercalation (d−f) of the first intercalated layer of MoS_2. Each image was acquired at a rate of 1 frame/s (data points, 512 × 512). The potential was swept from 3.2 V at a scan rate of 10 mV s^{-1}. The time indicated in each image started from the appearance of the new domain. The images of panels a−c were obtained at 1.25 V vs Li. Deintercalation (d−f) was observed at 1.35 V, when the current was also ca. 1−2 $\mu A\,cm^{-2}$. All images were taken in an area of 70 × 70 μm^2.

A new domain with a dark contrast appeared at the upper left side of Figure 4a and expanded, in the direction indicated by the arrow, into the inner part of the terrace. Another domain with the same dark contrast developed at the lower step (Figure 4b). The dark contrast ultimately became uniform throughout the terrace of interest (Figure 4c). Movie S1 in the Supporting Information captures the dynamic process in real time. Note that the yellow arrows show the relatively faster-growing direction only. The new domains were also expanding in other directions. Because the step edges were not always straight, which might have included kink sites, the intercalation reaction seems to be strongly dependent on the densities of kink sites at step edges. It is also expected that the intercalation reaction might be faster at kink sites than those at the straight steps. A further detailed analysis of growth rates is still under investigation. The absence of variations in the image contrast within the intercalated region strongly suggests that the intercalation initially proceeds within the first layer below the selvedge.

It has been reported that MoS_2 nanosheets with different thicknesses showed decrease in sheet resistances.[16] Therefore, it is expected that the first layer might be intercalated at the first stage. Simultaneous intercalation at the underlying layers would have produced domains of varying step heights. Furthermore, these results negate the possibility of Li-ion diffusion into the bulk of the material. If Fick's law of diffusion occurred across intercalated domains, the domain boundaries would have shown a gradual decrease in contrast. The acquired images indicated that the lithiated and delithiated domains led to the formation of two distinct phases. A similar phase separation was previously observed in the doping of Li with TiO_2.[30]

Previous experiments with LCM−DIM revealed that two adjacent terraces bordered by a step would appear as regions with the same intensity demarcated only by step lines; the sharp contrast at the step was an aftermath of the phase shift of two beams produced by the Nomarski prism at the step.[27] For this reason, LCM−DIM has been used for the detection of steps on the surface of a material where the upper and lower terraces have the same physical property. Monoatomic step heights, as small as 1.4 Å as in the case of Si(100), can be detected by LCM−DIM.[25] Thus, the interlayer distances of the individual sheets in MoS_2 (0.62 nm) and its lithiated form, $LiMoS_2$ (0.629 nm), might be discernible by the present optical technique.[13]

However, the images shown in Figure 4 did not show only steps as observed on Au(111) (described in previous works).[22,23] It is clear that new domains with different contrasts appeared during the intercalation reaction. MoS_2 shows absorption bands in the visible region.[15,16] Such absorption peaks are changed by the intercalation of Li ions.[12,31−33] It is reasonably expected that the appearance of different contrast in the intercalated regions are also caused by the difference of the adsorption spectra.

To the best of our knowledge, the present study is the first demonstration of a further ability of LCM−DIM to monitor contrast differences on the surface domains which might have been caused by the change in optical properties. Such significant demonstration creates further motivation to the researchers to investigate the in situ surface reactions caused by changes in optical properties in the monolayer regime. In addition to the present work, our ongoing surface investigation further focuses on the visualization of redox reactions in several organic monolayers. After the completion of the intercalation in the first layer below the selvedge, the potential was scanned in the positive direction and was set at 1.35 V, when the current density was only ca. 1−2 $\mu A\,cm^{-2}$. Figure 4d−f shows the restoration of the image contrast on the terrace as the Li ions were deintercalated. The rate of disappearance of the Li-intercalated domains was noticeably not uniform. A careful inspection of Movie S1 reveals that the intercalation from the upper left corner to the lower right corner seemed faster than that in other directions. The deintercalation reaction was also found to occur with different rates. This behavior can be ascribed to the direction along the *b*-axis in MoS_2.

The arrows in Figure 4 indicate the directions where the rate of the intercalation and deintercalation reactions were relatively faster than those in other directions. However, the presence of kink sites made the steps deviate from the straight path. Further work on the evaluation of the rate of reactions is still needed to understand this uniaxial process along the channels.

Significantly, the rate of reactions depends on the electrode potential as expected from Figure 1a. Note that in terraces shown in Figures 4 and 5 there were local variations in contrast. However, these contrasts were shown clearly by applying a high contrast in the data treatment to make a clear contrast difference between the doped and undoped areas. Therefore, the local variation in contrast seems to be artificial. If there were

DOI: 10.1021/jacs.5b11849
J. Am. Chem. Soc. 2016, 138, 3355−3361

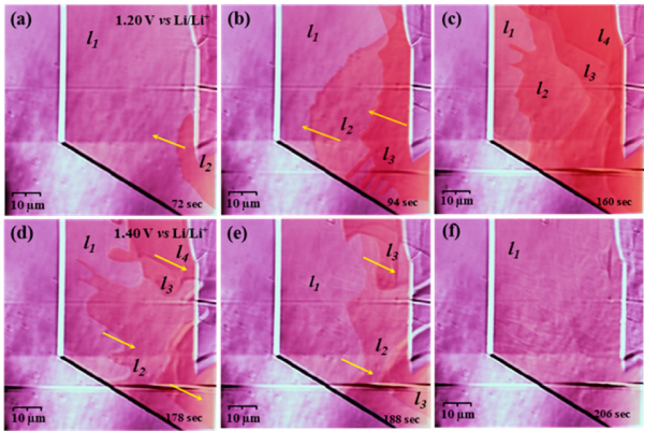

Figure 5. Dynamic processes of the intercalation and deintercalation reactions involving multilayers. After the intercalation of the first layer as shown in Figure 4c, the electrode potential was shifted to the anodic direction by only a few millivolts (2−3 mV). The second, third, and fourth layers marked by l_2, l_3, and l_4, respectively, started to be intercalated in a layer-by-layer mode (a−c). At more positive potentials (1.40 V), exhaustive deintercalation of the remnant layer transpired akin to the process captured in panels d−f. These layers exhibited different image contrasts, thereby allowing a distinct delineation of the intercalated and deintercalated domains (or phases). All images were taken in an area of 70 × 70 μm^2.

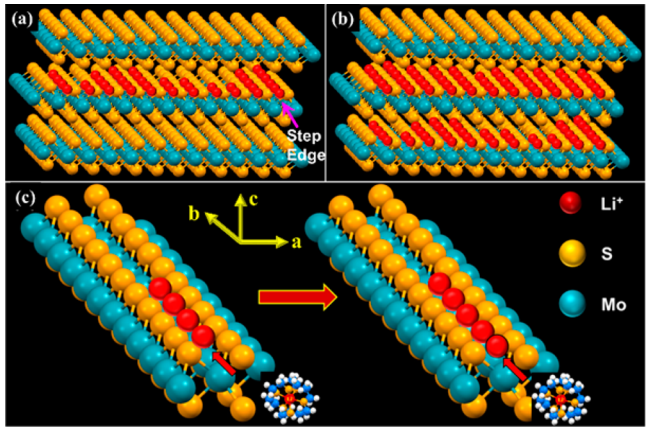

Figure 6. Illustrative depiction of the Li-ion intercalation of MoS_2 along the *b*-axis. The first layer underneath the selvedge is intercalated first to (near) completion prior to the intercalation of the second layer (a, b). A solvated Li ion is initially intercalated at the steps. All intercalated Li ions along the *b*-axis are pushed toward the interior of the crystal. In this example, a row of four intercalated Li ions takes in an incoming Li ion, making the row with five ions.

some defects, the reactions might have also started on terraces. Such modulations can be also seen in Figure 2a.

Intercalation and Deintercalation of Multilayers. After acquisition of the images shown in Figure 4, the electrode potential was swept in the negative direction (only 2−3 mV) to induce further intercalation. Figure 5a−c depicts the progressive intercalation of multilayers. Domain l_1 in Figure 5a represented the selvedge under which lay the first intercalated layer. The involvement of n underlying layers (where n = 2, 3, 4) triggered the emergence of other domains (l_n) with distinct image contrasts.

Figure 5 is one of the examples of the intercalation reactions. We expected that many steps might exist near the left lower corner or out of the observed area, which became reaction sites to form multilayers. In addition, along axes **a** and **b** shown in Figure 6, the samples have the equivalent crystal structure, which caused the two-dimensional growth of domains. These multilayers seemed to initiate from the lower right corners where we believe that reactions were also started from step edges located at these corners. The Supporting Information contains one more video (Movie S5) in which multilayer formations occurred in different directions of the intercalation. The corresponding deintercalation process was monitored in Figure 5d−f. Domain l_4 disappeared first; domains l_3 and l_2 followed. The deintercalation process occurred layer-by-layer, ultimately creating an atomically flat surface with Li ions still intercalated in the first monolayer underneath the selvedge. At more positive potentials, exhaustive deintercalation of the remnant layer transpired akin to the process captured in Figure 4d−f.

These processes are fully shown in Movie S2 in the Supporting Information. Figure 6 illustrates a proposed mechanism of the intercalation and deintercalation processes of Li ions in MoS_2 based on the images provided by in situ LCM−DIM.

For clarity of the mode, we drew the step edge as being straight without kink sites. In addition, the structural model in Figure 6 is shown along the **b** axis. It is located along the **a** and **b** axes at 120° angles to each other; the structure along the *b* axis should be the same as **a**. Therefore, the growth of domains should occur in two-dimensional diffusion. Moreover, the edges should have irregular shape, including many kink sites. These kink sites are expected to cause quasi-two-dimensional growth of domains as described above. (i) Li ions are initially incorporated at the steps of the MoS_2 crystal. (ii) Intercalated Li ions accumulate to form of a monatomic row along the **b** axis that moves toward the interior portion of the MoS_2 sheet. (iii) At the early stage of intercalation, Li ions occupy all available sites along the **b** axis, i.e., they do not readily diffuse to other sublayers. In effect, intercalated domains (or phases) are distinctly delineated from those that remain intercalant-free. (iv) Current densities for both intercalation and deintercalation almost linearly increased with potential. This suggests that the rate-determining process is not governed by Butler−Volmer kinetics but is an interplay of two factors: the charge-transfer process at the step and the force that pushes a row of Li ions into the interior of the basal plane of the crystal.

Extensive Intercalation Processes. Thus, far, the LCM−DIM images were acquired only at very low current densities (1−2 $\mu A\,cm^{-2}$) that induce intercalation and deintercalation within only a few monolayers from the MoS_2 selvedge. To reveal surface structural changes associated with high concentration of intercalated ions, the electrode potential was scanned until the peak current for intercalation reached ca. 12 $\mu A\,cm^{-2}$. The black trace in Figure 7a was obtained when the potential was scanned up to 1.0 V from the 2.5 V; included for comparison is the voltammogram in red trace similar to the one shown in Figure 1a. The cathodic peak at ca. 1.1 V was the signpost for intercalation; the anodic peak at 1.45 V marked the deintercalation process.

Figure 7b shows the voltammetric behavior of MoS_2 cycled repeatedly between 1.9 and 0.9 V. Coulometric analysis indicated that ca. 100−150 layers were involved. Currents for both intercalation and deintercalation increased with the number of potential cycles. The peak potentials for

DOI: 10.1021/jacs.5b11849
J. Am. Chem. Soc. 2016, 138, 3355−3361

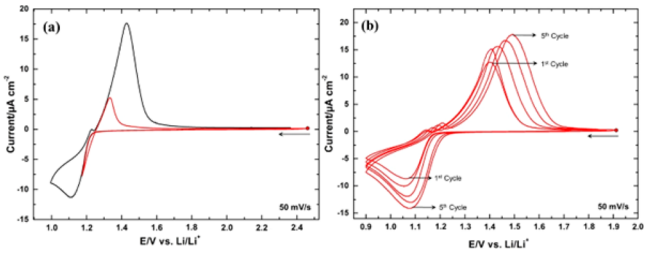

Figure 7. Current–potential profiles of MoS_2 extensively intercalated with Li ions. (a) The red trace shows the cyclic voltammogram of an initial stage of the intercalation reaction of ca. four layers. The black trace represents the cyclic voltammogram of a sample containing ca. 20 intercalated layers (total charge, ca. 4 mC cm^{-2}) prepared by expanding the potential window to 0.95 V. The peaks at 1.1 and 1.4 V correspond to the intercalation and deintercalation reactions, respectively. The scan rate for both traces is 50 mV s^{-1}. (b) Repeated voltammetric cycles between 0.9 and 1.9 V show that the currents progressively increased with increasing number of potential cycles.

deintercalation progressively shifted toward the positive direction. It is anticipated that the deintercalated Li ions in the deeper part of the crystal need larger overpotentials. The concomitant increase in the deintercalation current was ascribed to the proliferation of step sites that disrupted the atomically flat surface. Topographic details of this surface disruption are evident in the LCM–DIM images of Figure 8.

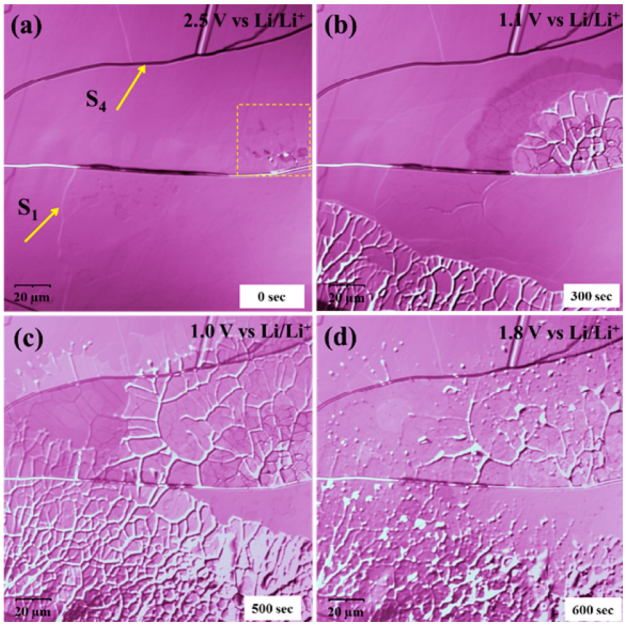

Figure 8. Surface evolution of MoS_2 as the potential was swept at a scan rate of 10 mV s^{-1}. (a) Initial state at 2.5 V. (b) At 1.1 V, which is the intercalation peak potential shown in the black trace of Figure 7a. (c) At 1.0 V, reticulated (netlike) features covered the surface. The deintercalation (d) was observed, and reticulation persisted even at 1.8 V. All images were taken in an area of 140 × 140 μm^2.

The initial surface in Figure 8a was strewn with multiple steps of different heights. The steps marked by S_1 were monatomic. A multiatomic step is denoted by S_4. The boxed-in area (Figure 8a) rapidly developed reticulated (netlike) features with variant contrasts, indicative of fast intercalation that involved underlying multilayers.

The reticulated domains spread throughout the surface, as can be seen in Figure 8b,c. Despite the reticulation, the intercalated layers appeared as dark domains, in a manner similar to what was observed at low intercalation current densities. The total amount of charge was 3 mC cm^{-2} at the stage shown in Figure 8c.

The growth of fronts of the smooth multilayer and the netlike structures occurs at similar speed. However, a careful inspection indicates that the local growth rates were different. Interestingly, it was also found that further formation of netlike structures was observed more clearly. Similar netlike features have been observed on layered surfaces during metal deposition and intercalation in ultrahigh vacuum.[10,11,34–36] This behavior has been interpreted by a lattice expansion of the surface layers.[34–36] We are now studying the netlike structures more carefully in electrochemical conditions by changing the electrode potential.

The bright veins of the reticulation suggested that Li ions existed in multilayers along these lines. After the acquisition of the image in Figure 8c, the electrode potential was scanned to anodic direction at 50 mV s^{-1} to spur deintercalation. Many of the intercalated domains gradually disappeared with concomitant changes in contrast similar to those of Figure 4. However, the reticulation persisted even after 15 min at 1.8 V, as shown in Figure 8d. Movie S3 shows these processes.

Finally, the electrode potential was stepped from 1.7 to 0.9 V. The intercalation reaction occurred at a rapid rate. Movie S4 shows an example acquired during such a fast intercalation reaction. Each image was acquired 0.25 s/frame (data points, 256 × 256). It is clear that such experiments demonstrated that our LCM–DIM can follow the fast electrochemical reactions. Note that the current at 0.9 V was ca. 10 μA cm^{-2}, which was almost constant for 10 min. The growth of fronts of the smooth multilayer and the netlike structures was also seen, as shown in Figure 8. However, the rate of the expansion of intercalated smooth domains was roughly 10–15 times larger than that found in Figure 4, because the current at 0.9 V is larger than that in Figure 4. The reticulated domains presumably started at defect sites and also spread rapidly. Note that the shape of the reticulated domains seems to be different from those found in Figure 8, suggesting that the lattice expansion depends on the electrode potential. More detailed study is now under investigation.

Finally, it is noteworthy that the intercalation and deintercalation reactions could be imaged for graphite materials, which suggests that LCM–DIM is a general method applicable to many battery electrodes.

CONCLUSIONS

In situ images of the dynamic intercalation of Li ions into MoS_2 single-crystal electrodes were acquired for the first time, under potential control, with the use of a technique combining laser confocal microscopy with differential interference microscopy. Analysis of variations in the image contrast provided a visual indicator that differentiated the intercalated domains from the intercalant-free regions. Li ions initially occupied the steps and proceeded to form channels within the MoS_2 crystal in a layer-by-layer fashion. Within an appreciable potential window between 0.9 and 1.8 V, the rate-determining step of the intercalation and deintercalation processes was not governed by Butler–Volmer kinetics. Newly inserted Li ions were pushed atom-by-atom into the channels to form wide domains. The intercalation and deintercalation processes were chemically

DOI: 10.1021/jacs.5b11849
J. Am. Chem. Soc. 2016, 138, 3355–3361

reversible and could be repeated many times within a few atomic layers. However, extensive intercalation of Li ions led to the disruption of the atomically flat surface as evidenced by reticulated surface features that developed into cracks that ultimately peeled off from the surface. The demonstrated capability of LCM−DIM ushers in new possibilities for the direct observation of surface reactions accompanied by changes in optical properties in the monolayer regime.

■ ASSOCIATED CONTENT

Supporting Information

The Supporting Information is available free of charge on the ACS Publications website at DOI: 10.1021/jacs.5b11849.

Experimental procedure, additional experimental results, captions for Movies S1−S5(PDF)
Movie S1 (AVI)
Movie S2 (AVI)
Movie S3 (AVI)
Movie S4 (AVI)
Movie S5 (AVI)

■ AUTHOR INFORMATION

Corresponding Author

*itaya@atom.che.tohoku.ac.jp

Notes

The authors declare no competing financial interest.

■ ACKNOWLEDGMENTS

The authors acknowledge Prof. G. Sazaki (Hokkaido University), Mr. Y. Saito (Olympus), and Mr. S. Kobayashi (Olympus) for developing and improving the LCM−DIM system. The authors are grateful to Prof. M. Soriaga and Dr. J. Baricuatro (Joint Center for Artificial Photosynthesis, California Institute of Technology, Pasadena, United States) for their helpful suggestions and discussion of the paper. This work was supported by the Ministry of Education, Culture, Sports, Science and Technology of Japan under Grant 20245038 and in part by the New Energy and Industrial Technology Development Organization (NEDO).

■ REFERENCES

(1) Gewirth, A. A.; Niece, B. K. *Chem. Rev.* **1997**, *97*, 1129.
(2) Itaya, K. *Prog. Surf. Sci.* **1998**, *58*, 121.
(3) Kolb, D. M. *Angew. Chem., Int. Ed.* **2001**, *40*, 1162.
(4) Yoshimoto, S.; Itaya, K. *Annu. Rev. Anal. Chem.* **2013**, *6*, 213.
(5) Itaya, K. *Electrochemistry* **2015**, *83*, 670.
(6) Więckowski, A. *Interfacial Electrochemistry: Theory, Experiment, and Applications*; Marcel Dekker: New York, 1999.
(7) Alliata, D.; Kötz, R.; Haas, O.; Siegenthaler, H. *Langmuir* **1999**, *15*, 8483.
(8) Inaba, M.; Kawatate, Y.; Funabiki, A.; Jeong, S.-K.; Abe, T.; Ogumi, Z. *Electrochim. Acta* **1999**, *45*, 99.
(9) Campana, F. P.; Kötz, R.; Vetter, J.; Novák, P.; Siegenthaler, H. *Electrochem. Commun.* **2005**, *7*, 107.
(10) Dora, S. K.; Bai, Y.; Elbahri, M.; Kunz, R.; Adelung, R.; Magnussen, O. *J. Electrochem. Soc.* **2008**, *155*, D666.
(11) Dora, S. K.; Magnussen, O. *J. Electrochem. Soc.* **2008**, *155*, F132.
(12) Benavente, E.; Santa Ana, M. A.; Mendizábal, F.; González, G. *Coord. Chem. Rev.* **2002**, *224*, 87.
(13) Stephenson, T.; Li, Z.; Olsen, B.; Mitlin, D. *Energy Environ. Sci.* **2014**, *7*, 209.
(14) Fang, X.; Hua, C.; Guo, X.; Hu, Y.; Wang, Z.; Gao, X.; Wu, F.; Wang, J.; Chen, L. *Electrochim. Acta* **2012**, *81*, 155.
(15) Lacey, S. D.; Wan, J.; Cresce, A. v. W.; Russell, S. M.; Dai, J.; Bao, W.; Xu, K.; Hu, L. *Nano Lett.* **2015**, *15*, 1018.
(16) Xiong, F.; Wang, H.; Liu, X.; Sun, J.; Brongersma, M.; Pop, E.; Cui, Y. *Nano Lett.* **2015**, *15*, 6777.
(17) Wen, R.; Rahn, B.; Magnussen, O. M. *Angew. Chem., Int. Ed.* **2015**, *54*, 6062.
(18) Magnussen, O. M.; Polewska, W.; Zitzler, L.; Behm, R. J. *Faraday Discuss.* **2002**, *121*, 43.
(19) Andersen, J. E. T.; Bech-Nielsen, G.; Møller, P.; Reeve, J. C. *J. Appl. Electrochem.* **1996**, *26*, 161.
(20) Divisek, J.; Steffen, B.; Stimming, U.; Schmickler, W. *J. Electroanal. Chem.* **1997**, *440*, 169.
(21) Van Driessche, A. E. S.; Otálora, F.; Sazaki, G.; Sleutel, M.; Tsukamoto, K.; Gavira, J. A. *Cryst. Growth Des.* **2008**, *8*, 4316.
(22) Wen, R.; Lahiri, A.; Azhagurajan, M.; Kobayashi, S.-i.; Itaya, K. *J. Am. Chem. Soc.* **2010**, *132*, 13657.
(23) Azhagurajan, M.; Wen, R.; Lahiri, A.; Kim, Y. G.; Itoh, T.; Itaya, K. *J. Electrochem. Soc.* **2013**, *160*, D361.
(24) Wen, R.; Lahiri, A.; Alagurajan, M.; Kuzume, A.; Kobayashi, S.-i.; Itaya, K. *J. Electroanal. Chem.* **2010**, *649*, 257.
(25) Kobayashi, S.-I.; Kim, Y.-G.; Wen, R.; Yasuda, K.; Fukidome, H.; Suwa, T.; Kuroda, R.; Li, X.; Teramoto, A.; Ohmi, T.; Itaya, K. *Electrochem. Solid-State Lett.* **2011**, *14*, H351.
(26) Azhagurajan, M.; Wen, R.; Kim, Y. G.; Itoh, T.; Sashikata, K.; Itaya, K. *Surf. Sci.* **2015**, *631*, 57.
(27) Sazaki, G.; Matsui, T.; Tsukamoto, K.; Usami, N.; Ujihara, T.; Fujiwara, K.; Nakajima, K. *J. Cryst. Growth* **2004**, *262*, 536.
(28) Sugimoto, T.; Atsumi, Y.; Kikuta, M.; Ishiko, E.; Kono, M.; Ishikawa, M. *J. Power Sources* **2009**, *189*, 802.
(29) David, L.; Bhandavat, R.; Barrera, U.; Singh, G. *Sci. Rep.* **2015**, *5*, 9792.
(30) Wagemaker, M.; van de Krol, R.; Kentgens, A. P. M.; van Well, A. A.; Mulder, F. M. *J. Am. Chem. Soc.* **2001**, *123*, 11454.
(31) Acrivos, J. V.; Liang, W. Y.; Wilson, J. A.; Yoffe, A. D. *J. Phys. C: Solid State Phys.* **1971**, *4*, L18.
(32) Papageorgopoulos, C. A.; Jaegermann, W. *Surf. Sci.* **1995**, *338*, 83.
(33) Wang, Y.; Ou, J. Z.; Chrimes, A. F.; Carey, B. J.; Daeneke, T.; Alsaif, M. M. Y. A.; Mortazavi, M.; Zhuiykov, S.; Medhekar, N.; Bhaskaran, M.; Friend, J. R.; Strano, M. S.; Kalantar-Zadeh, K. *Nano Lett.* **2015**, *15*, 883.
(34) Adelung, R.; Ernst, F.; Scott, A.; Tabib-Azar, M.; Kipp, L.; Skibowski, M.; Hollensteiner, S.; Spiecker, E.; Jäger, W.; Gunst, S.; et al. *Adv. Mater.* **2002**, *14*, 1056.
(35) Adelung, R.; Hartung, W.; Ernst, F. *Acta Mater.* **2002**, *50*, 4925.
(36) Spiecker, E.; Schmid, A. K.; Minor, A. M.; Dahmen, U.; Hollensteiner, S.; Jäger, W. *Phys. Rev. Lett.* **2006**, *96*, 086401.

DOI: 10.1021/jacs.5b11849
J. Am. Chem. Soc. 2016, 138, 3355−3361